Validation of the GROMOS 54A7 Force Field Regarding Mixed *α*/*β*-Peptide Molecules

by **Dongqi Wang**[a]), **Fabian Freitag**[a]), **Zrinka Gattin**[a]), **Hannah Haberkern**[a]), **Bernhard Jaun**[b]), **Magdalena Siwko**[a]), **Rounak Vyas**[a]), **Wilfred F. van Gunsteren***[a]), and **Jožica Dolenc***[a])

[a]) Laboratory of Physical Chemistry, Swiss Federal Institute of Technology, ETH, CH-8093 Zürich (phone: +41446325501; fax: +41446321039; e-mail: wfvgn@igc.phys.chem.ethz.ch, jozi@igc.phys.chem.ethz.ch)

[b]) Laboratory of Organic Chemistry, Swiss Federal Institute of Technology, ETH, CH-8093 Zürich

Dedicated to Prof. *Dieter Seebach* on the occasion of his 75th birthday

A molecular-dynamics (MD) simulation study of two heptapeptides containing α- and β-amino acid residues is presented. According to NMR experiments, the two peptides differ in dominant fold when solvated in MeOH: peptide **3** adopts predominantly β-hairpin-like conformations, while peptide **8** adopts a *14*/*15*-helical fold. The MD simulations largely reproduce the experimental data. Application of NOE atom–atom distance restraining improves the agreement with experimental data, but reduces the conformational sampling. Peptide **3** shows a variety of conformations, while still agreeing with the NOE and ^3J-coupling data, whereas the conformational ensemble of peptide **8** is dominated by one helical conformation. The results confirm the suitability of the GROMOS 54A7 force field for simulation or structure refinement of mixed α/β-peptides in MeOH.

Introduction. – The introduction of β-residues into α-peptides, either sequentially or alternatively, yields α/β-mixed peptides, which show similar properties as β-peptides and have the potential to be used in pharmaceutical industry [1–5]. Their unique properties include the strong propensity to fold into stable secondary structures [1][3][6–8], and their *in vivo* and *in vitro* resistance to proteases [9]. Particular sequences of α- and β-residues in α/β-mixed peptides have been found to lead to new types of secondary structure [8][10–15] which evoked a growing interest in experimental as well as theoretical investigations of peptide–protein interactions using such peptides in order to mimic protein–protein interactions [16].

In general, experimental methods capture the average values over time and molecules of particular quantities, *e.g.*, from NMR experiments, or a specific molecular geometry as in a crystal matrix, *e.g.*, from X-ray diffraction. This averaging induces a loss of information on the molecular conformations along a trajectory, thus the model structures derived from the observed values of particular quantities on the basis of particular mathematical models and procedures do not provide a complete picture of the dynamics of the system. This limitation of experimental techniques may be compensated by means of theoretical studies with appropriate computation models, such as molecular dynamics (MD) simulation based on classical force fields [17–19] which can provide details on the conformational and energetic changes of the molecules as a function of time, for example, on the folding/unfolding behavior of a

peptide, or first-principle quantum-chemical models [20–22] which may provide a high-resolution molecular picture by explicitly including the contribution of electronic degrees of freedom to the molecular energy. The former are the methods of choice compared to the latter when dealing with slow processes in large systems, *e.g.*, polypeptide folding equilibria, in view of a reasonable compromise between accuracy and computational cost. Indeed, force-field based biomolecular simulation has been shown to be a powerful tool in studying biological and pharmacochemical processes on a molecular level [23–29], and can simulate conformational and time-dependent properties, and thus provide mechanistic insights towards a better understanding of particular processes, from which one may infer and propose rational modifications of existing compounds towards a special purpose.

The present study concerns the validation of the latest version, 54A7 [30][31] of the GROMOS force field [32] by means of the simulation of two mixed α/β-peptides for which NMR NOEs and $^3J(H_N,H_{\alpha/\beta})$ couplings are available [16]. In a previous validation study using two β-peptides [33], the 54A7 force field was found to stabilize the helical conformations of these peptides, and to reproduce the folding equlibria slightly better than the earlier versions 53A6 [34] and 45A3 [35] of the GROMOS force fields.

In the present study, we used two mixed α/β-peptides [16] as model systems, H-(*S*)-β^2hLeu-Ile-(*S*)-β^2hMet-Lys-(*S*)-β^2hVal-Ala-(*S*)-β^2hPhe-OH (compound **3** from [16]) and H-(*S*)-β^3hLeu-Aib-(*R*)-β^3hVal-Aib-(*S*)-β^3hAla-Aib-(*S*)-β^3hPhe-OH (compound **8** from [16]; see *Fig. 1*). According to the single-structure refinement based on NOE distance-bound restraining, these two peptides display in MeOH novel types of secondary structure with **3** adopting a hairpin turn closed by a nine-membered H-

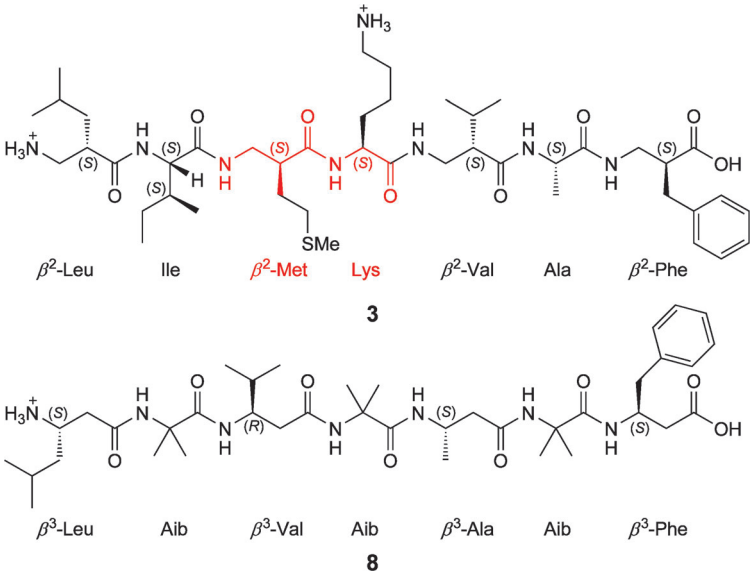

Fig. 1. *The two peptides* **3** *and* **8** *from* [16]. The residues in red were reported to adopt a hairpin turn forming a nine-membered ring closed by the H-bond β^2Met3 H:Lys4O.

bonding ring and **8** adopting a *14*/*15* helix with its corresponding H-bonds. We note that many factors may contribute to the stability of particular secondary structure of peptides in solution [27], among which are intramolecular H-bonding, *Van der Waals* interactions, the hydrophobic effect, and other solvation effects. The relative weights of these contributions are determined by the composition of the solute, its geometric features, distribution of polar moieties, and the polarity of the solvent. A particular force-field parameter set represents a particular combination of these factors. In case an MD simulation based on a particular force field does not reproduce the experimental data available for the peptide, this force-field deficiency may be redressed by restraining the motion of the peptide such that the experimental data are reproduced. Experimentally, NOE distance bounds are obtained as averages over an ensemble, thus the atom–atom distance restraining should be imposed on average on a series of molecular structures or a trajectory [36].

In the present study we report four simulations, two for each peptide, one without and one with NOE distance-bound restraining in the simulation.

Computational Details. – The two peptides, compounds **3** and **8** from [16], and solvent were modeled using the GROMOS force field 54A7 [30][31]. The MeOH solvent molecules were modeled using a rigid three-site model [37]. Aliphatic CH_n groups ($n = 1-3$) were treated as united atoms, both in the solute and solvent. The Lys residue and the N- and C-termini of the peptides were protonated, and Cl^- anions were added to neutralize the solute charge (2 for **3** and 1 for **8**). One of the ten model structures derived for each peptide from the NMR data [16] was taken as the initial structure for the molecular-dynamics (MD) simulations. The unrestrained MD simulations covered 80 ns. In the restrained MD simulations, the 38 atom–atom distance bounds for peptide **3** (Table S1[1])) and the 53 atom–atom distance bounds for peptide **8** (Table S2[1])) were used as time-averaged distance restraints [36]. The parameters of distance-restraining potential energy term [38] were $k_{dr} = 1000$ kJ mol^{-1} nm^{-2} and $\tau_{dr} = 5$ ps. The distance-restrained simulations covered 40 ns. The trajectory configurations were saved every 1 ps.

Rectangular periodic boundary conditions were applied. The leap-frog algorithm was used to integrate *Newton*'s equations of motion with a time step of 2 fs. All bond lengths and the bond angle in MeOH were constrained to their ideal values using the procedure SHAKE [39] with a geometric precision of 10^{-4}. Long-range electrostatic interactions were handled with a triple-range cutoff scheme with cutoff radii of 0.8 nm (interactions updated every time step) and 1.4 nm (interactions updated every five-time steps). The mean effect of omitted electrostatic interactions beyond the long-range cutoff distance (1.4 nm) was accounted for by the inclusion of a *Barker–Watts* reaction-field force [40][41] based on a permittivity of 18 for MeOH [37]. The weak-coupling method [42] was used for keeping the temp. (300 K) and pressure (1 atm) constant, using coupling times $\tau_T = 0.1$ ps, $\tau_P = 0.5$ ps, and an isothermal compressibility of 1.6×10^{-3} kJ^{-1} mol nm^3 [37]. Solute and solvent degrees of freedom were separately coupled to the heat bath.

The analysis of trajectories was similar to that in previous work [19]. Atomic positional root-mean-square differences (RMSDs) were calculated for MD trajectory structures with respect to the first NMR model structure of [16]. The criterion used in the H-bond analysis was 0.25 nm as upper bound of the H $\cdots$ A (A: acceptor) distance and 135° as lower bound of the D $\cdots$ H $\cdots$ A angle (D: donor). A conformational cluster analysis [43] was carried out on the separate and combined trajectories of the peptides using structures at 5-ps intervals and using as backbone atom-positional RMSD similarity criterion 0.1 nm. The 38 and 53 available proton–proton distance bounds (Tables S1 and S2[1])), derived from measured NOE cross-peak intensities [16], were compared to averages over the whole trajectories calculated as $\langle r^{-6} \rangle^{-1/6}$. The H $\cdots$ H distances involving aliphatic H-atoms were calculated by defining virtual (CH_1), prochiral (stereospecific CH_2), and *pseudo* (Me and non-stereospecific CH_2) atomic

[1]) *Supplementary Material* is available from the corresponding authors.

positions, and the distance bounds for the latter were modified to include *pseudo*-atom distance bound corrections [44], the values of which were taken from [45]. ^3J-Coupling constants were calculated for the simulated and NMR model structures using the *Karplus* relation [46][47]

$$^3J(H_N, H_{\alpha/\beta}) = a\cos^2\theta + b\cos\theta + c$$

where θ is the dihedral angle between the planes defined by the atoms H, N, and $C_{\alpha/\beta}$, and the atoms N, $C_{\alpha/\beta}$, and $H_{\alpha/\beta}$. We calculated $^3J(H_N,H_{\alpha/\beta})$ coupling constants as a function of the backbone angle ϕ(C–N–C_α–C) for an α-residue and ϕ(C–N–C_β–C_α) for a β-residue using a phase shift $\delta = -60°$, which relates the torsional angles ϕ'(H_N–N–C_α–H_α) and ϕ'(H_N–N–C_β–H_β) to ϕ through $\phi' = \phi + \delta$. Only for $^3J(H_N,H_\beta^{si})$ of residue β^2-Leu3 $\delta = +60°$. The parameters *a*, *b*, and *c* were 6.4, −1.4, and 1.9 Hz, resp. [48].

The exper. data [16] which are used in the force-field validation were 38 H–H NOE distance bounds and nine $^3J(H_N,H_{\alpha/\beta})$ coupling constants for compound **3**, and 53 H–H NOE distance bounds and three $^3J(H_N,H_{\alpha/\beta})$ coupling constants for compound **8**, and are specified in Tables S1–S3 of *Supporting Information*[1]), together with the corresponding distance and ^3J-value averages obtained from the MD simulations and the sets of NMR model structures. These sets of NMR model structures, ten for each peptide, had been obtained [16] by single-structure refinement using simulated temp. annealing with the program XPLOR.

Results and Discussion. – 1. *Comparison to Experimentally Derived NOE Atom–Atom Distance Bounds.* The difference between the $< r^{-6} >^{-1/6}$ averaged H···H distances and the experimentally derived NOE distance bounds for the 38 NOEs observed for compound **3** are shown in *Fig. 2* and Table S1[1]) for the two MD simulations and for the set of ten NMR model structures [16]. In the unrestrained simulation of compound **3**, three NOE distance-bound violations larger than 0.1 nm are observed for the proton pairs Ile2:HA-β^2Val5:HA (0.28 nm, NOE 35), β^2Met3:HN-β^2Val5:HA (0.14 nm, NOE 37), and Lys4:HN-Ile2:HA (0.17 nm, NOE 38). These pairs involve distances that define alternative configurations of the residues involved in the β-turn, and the NMR model structures also show slight violations of these NOE bounds. As expected, the application of NOE distance restraining improves the agreement with NOE distance bounds, although the last bound is still slightly violated.

Fig. 3 shows the NOE distance-bound violations for the 53 NOE bounds in the two MD simulations, of compound **8** and for the set of ten NMR model structures [16]. In the unrestrained simulation, there are two violations larger than 0.1 nm, β^3Leu1:HB-β^3Ala5:HB (0.13 nm, NOE 42), and β^3Leu1:HD-β^3Ala5:HB (0.18 nm, NOE 43), both of which involve protons from the N-terminal residue (β^3Leu1), of which the amide H-atom is not involved in the *i* to *i* – 4 H-bonds that characterize the *14/15*-helical structure. This residue enjoys thus configurational freedom. Of the NOE bounds that are slightly violated in the NMR model structures [16] β^3Ala5 Aib4:H (0.06 nm, NOE 32), β^3Leu1:HB-Aib4:H (0.05 nm, NOE 41), and β^3Leu1:HD-β^3Ala5:HB(0.05nm, NOE 43), the latter two involve the N-terminal residue too. When applying NOE distance-bound restraining, no violation larger than 0.04 nm is observed.

2. *Comparison to Measured* ^{3}J-*Coupling Constants.* Experimentally, nine ^3J-coupling constants (H_N, H_β or H_N, H_α) for compound **3** and three for compound **8** are available from ^{1}H-NMR spectra [16]. The average values for these ^3J-coupling constants were calculated using the *Karplus* equation from the MD trajectories and for the sets of NMR model structures. The results for compounds **3** and **8** are presented in

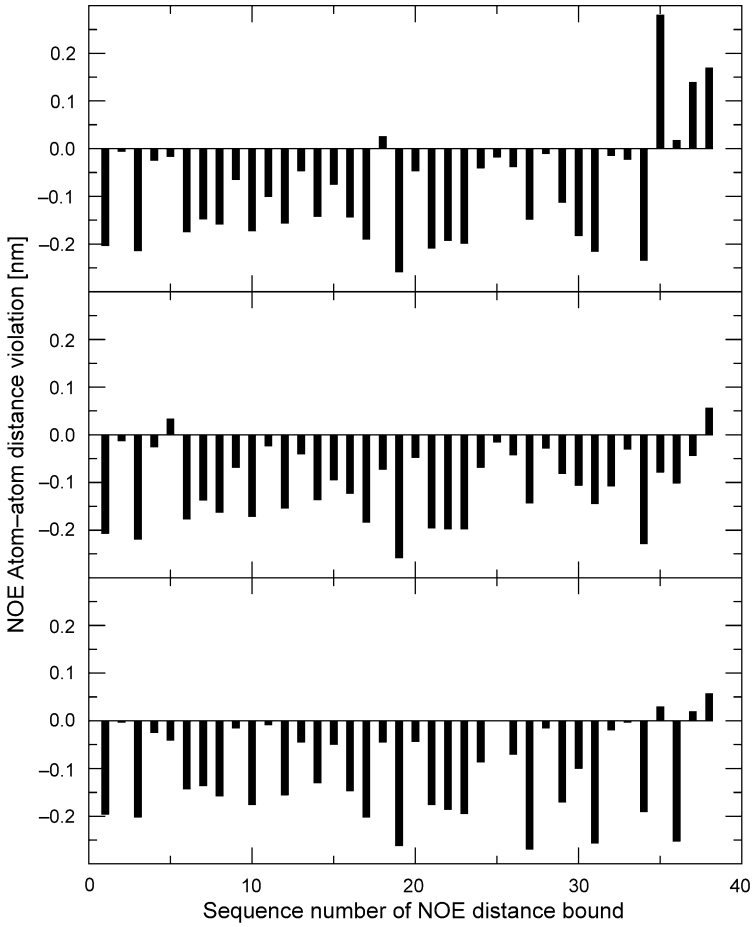

Fig. 2. *Compound* **3***: NOE distance-bound violations in the unrestrained* (upper panel) *and in the NOE distance-restrained* (middle panel) *MD simulations, and in the set of ten NMR model structures from* [16] (lower panel). The bounds are specified in Table S1[1]).

Fig. 4 and Table S3[1]). Since the *Karplus* relation offers a rather poor representation of the relation between ^3J value and the configuration of the atoms involved [49], differences up to 2 Hz do not represent significant deviations between model and experiment. Almost all of the calculated values fall within the ± 2 Hz range from the experimental value. For peptide **3**, the application of NOE distance restraints does not improve the agreement with experiment, while for peptide **8** it does marginally.

3. *Structural Characterization of Compounds* **3** *and* **8**. *Fig. 5* shows the backbone atom-positional RMSDs of the MD trajectory structures from the NMR model (hairpin or helical) structure that was used as initial structure for the two peptides as a function of simulation time. In the unrestrained simulation of compound **3**, conformations different from the NMR model dominate the trajectory, during most of the simulation time the RMSD is larger than 0.2 nm. However, after 70 ns the RMSD is comparable to

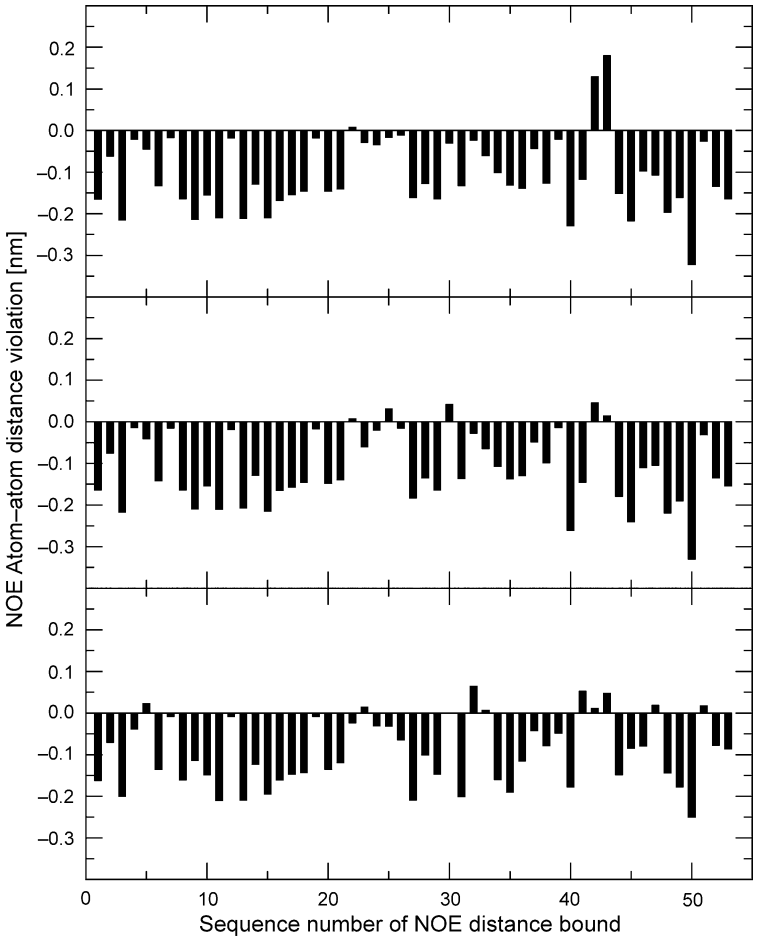

Fig. 3. *Compound* **8***: NOE distance-bound violations in the unrestrained* (upper panel) *and in the NOE distance-restrained* (middle panel) *MD simulations, and in the set of ten NMR model structures from* [16] (lower panel). The bounds are specified in Table S2[1]).

the one in the NOE-restrained simulation. Application of NOE distance-bound restraining leads to smaller RMSD values than in the unrestrained simulation. In the unrestrained simulation of compound **8**, folding-unfolding transitions are observed, and the residence time of the helical folded conformations can be as long as 20 ns, suggesting a clear preference for a helical folding mode. The use of NOE distance-bound restraining enhances this preference, and the simulation is hardly sampling unfolded conformations.

The occurrence of H-bonds in the simulation of compound **3** is displayed in *Supporting Information* (Fig. S1[1])). In the unrestrained simulation, there is one H-bond (*ca.* 38% of the simulation) or none at all (*ca.* 35%). The two most populated H-bonds, between atom pairs β^2Phe7:HN-β^2Leu1:O and β^2Met3:HN-β^2Val5:O, emerge only

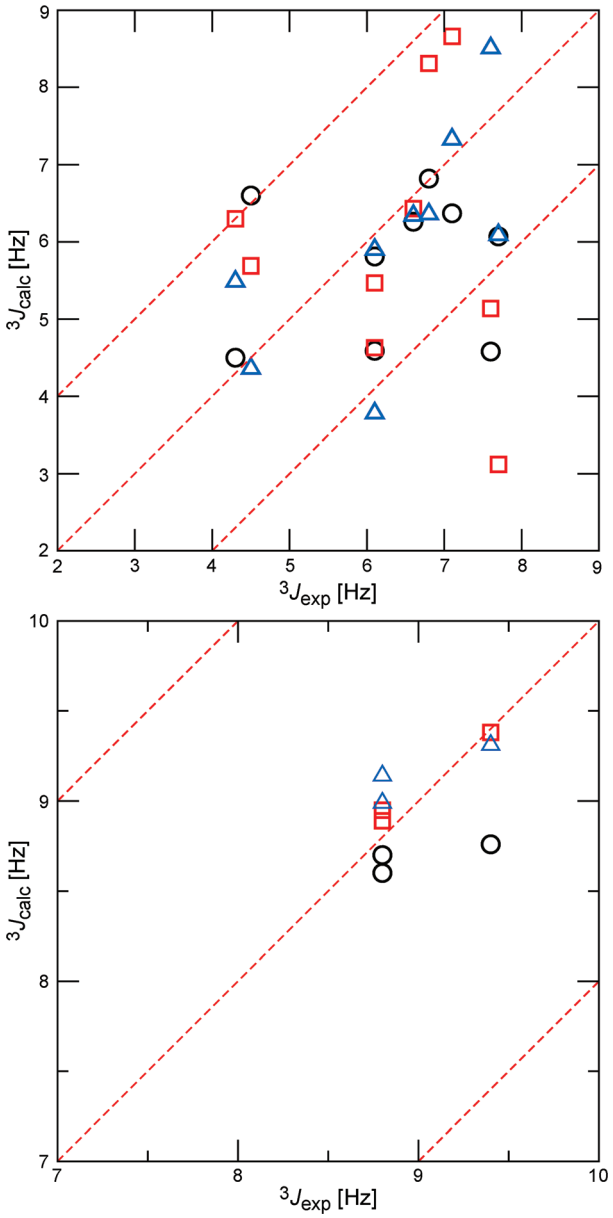

Fig. 4. *Average* $^3J(H_NH_{\alpha/\beta})$ *coupling constants of compounds* **3** (upper panel) *and* **8** (lower panel), *and the corresponding measured values* [16]. *Circles:* unrestrained MD simulations. *Squares:* NOE distance-bound restrained MD simulations. *Triangles:* NMR model structures [16]. The values are specified in Table S3[1]).

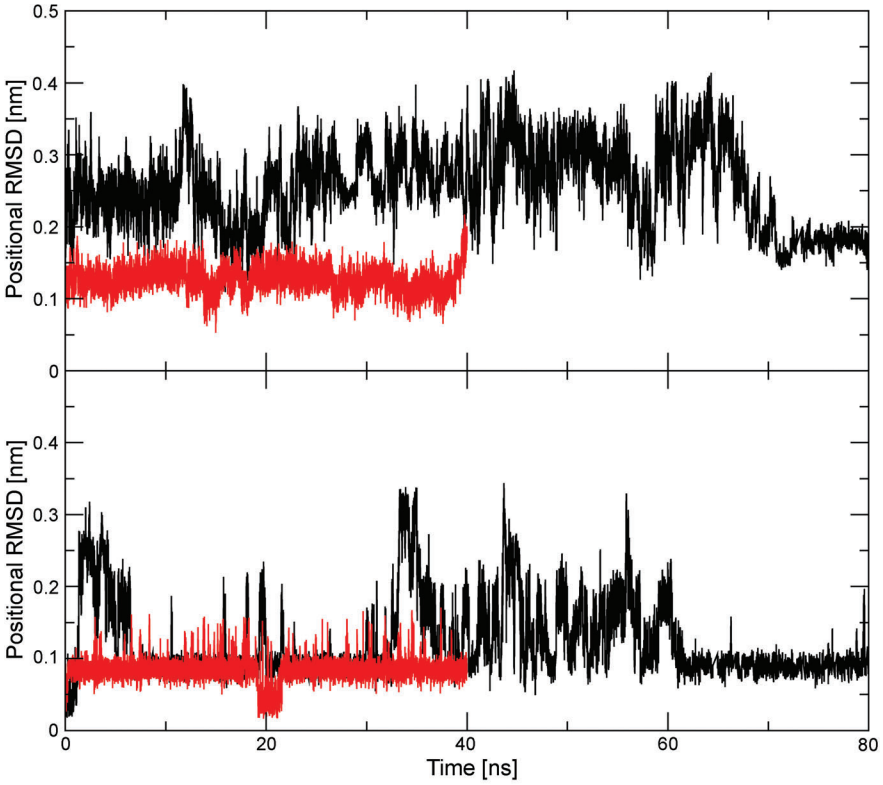

Fig. 5. *Positional RMSD of non-terminal backbone atoms of compounds* **3** (upper panel) *and* **8** (lower panel) *with respect to the NMR model structure* [16] *that was used as initial structure. Black:* unrestrained MD simulations. *Red:* NOE distance-restrained simulations.

after 70 ns and have populations of 10–13%. NOE Distance-bound restraining changes the tendency to form H-bonds. During most of the simulation, there is one (*ca.* 62% of the simulation time) or no (*ca.* 27%) H-bonds. The most populated H-bond is Ala6:HN-β^2Leu1:O (57%). However, we did not observe the H-bond β^2Met3:HN-Lys4:O that closes a nine-membered ring. Even when NOE distance restraints are applied, the force field does not favor the formation of this H-bond.

In the case of compound **8** (see *Supporting Information*, Fig. S2[1]), the dominant H-bonds, β^3Phe7:HN-β^3Val3:O (55%), Aib6:HN-Aib2:O (58%), and β^3Ala5:HN-β^3Leu1:O (46%), are of type *i* to *i* – 4 characterizing a *14*/*15*-helical structure as reported in the experimental study. The restraining with NOE distance bounds enhances the presence of these H-bonds, their occurrences increasing to 65, 82, and 81%, respectively.

Conformational clustering analysis can be used to determine the variation in conformations in a trajectory or set of structures, and when combining two trajectories or sets of structures to determine the degree of overlap between the configurations sampled.

As seen in *Fig. 6*, the population of the major conformational cluster in the simulations of compound **3** is 11 and 44% for the unrestrained and NOE restrained cases, respectively. As expected, the NOE distance-bound restraining slightly reduced

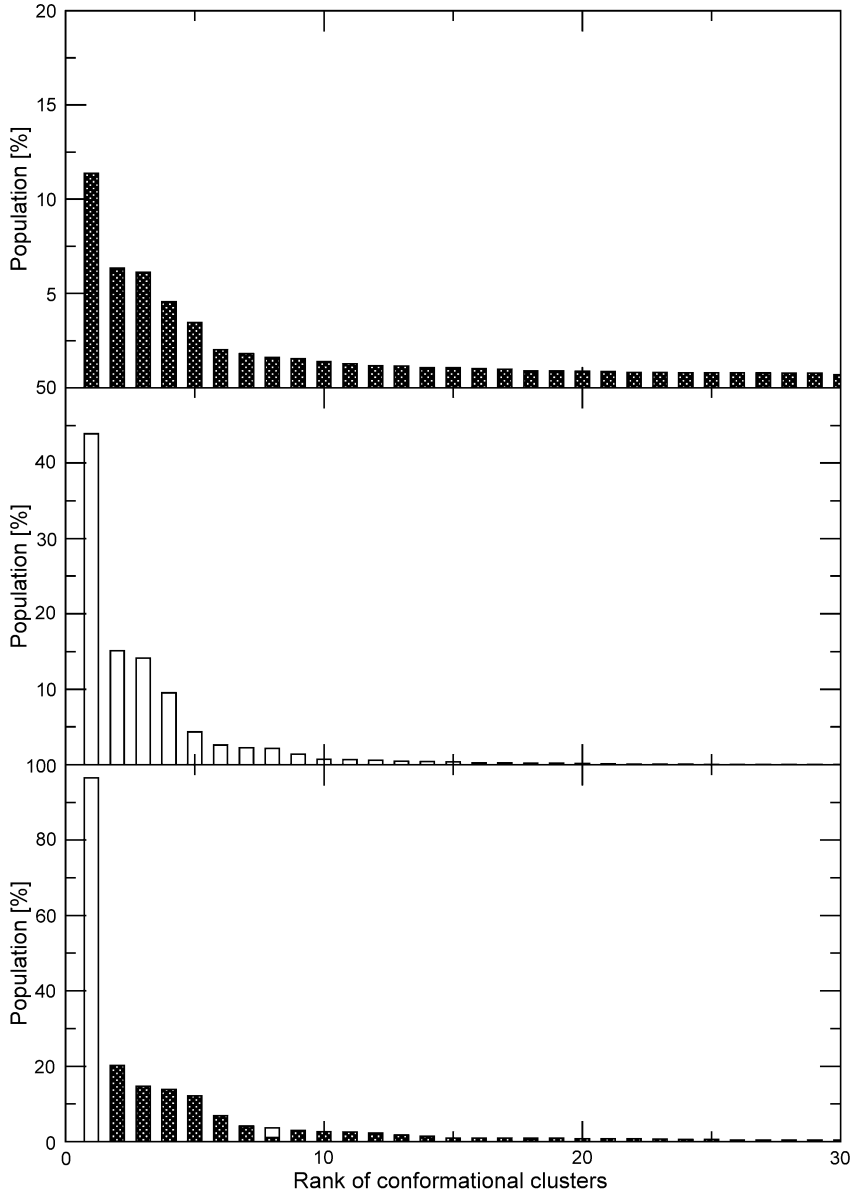

Fig. 6. *Compound* **3**: *conformational clustering of the 80-ns trajectories of the unrestrained simulation* (upper panel), *40-ns trajectories of the NOE-restrained simulation* (middle panel), *and of the combined trajectory consisting of the 80-ns-long unrestrained and 2 × 40 ns restrained simulations* (lower panel)

the conformational space of compound **3** sampled within 80 ns. The number of clusters that make up 99% of the trajectory at 40 ns is decreased from *ca*. 250 to 37 (see *Fig. 7*). The lowest panel of *Fig. 6* shows that the conformational space sampled in the two simulations does not show much overlap. The unrestrained and NOE-restrained simulations have sampled different conformations, which is consistent with the observations in the analysis of the atom-positional RMSD from the initial structure in *Fig. 5* and the H-bond analysis in Fig. S1[1]). This is also illustrated by the conformations of the central structures of the most populated clusters in the two simulations shown in *Figs. 8* and *9*.

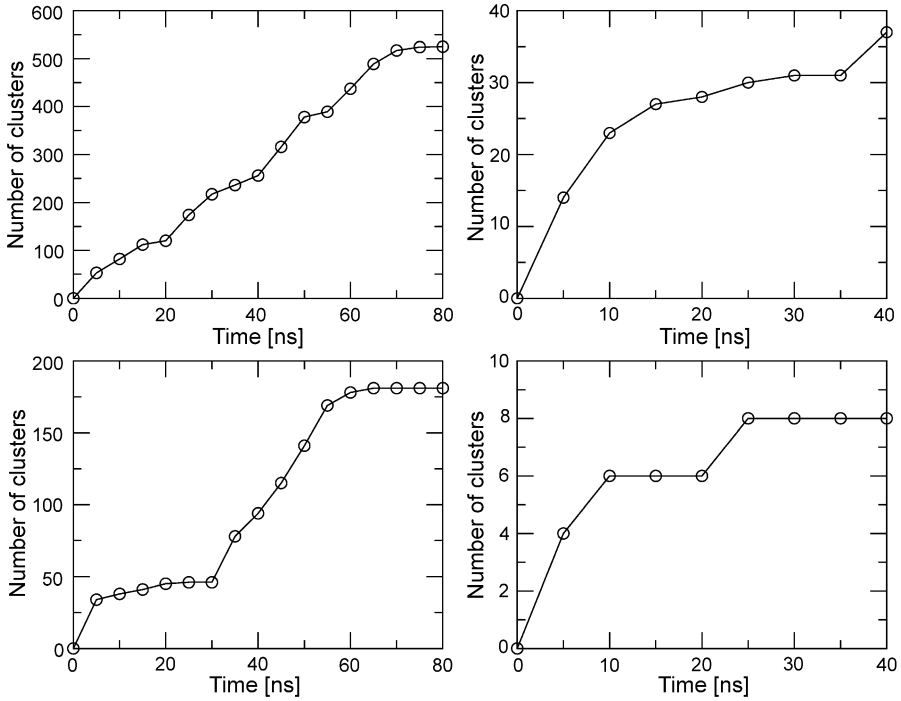

Fig. 7. *Number of conformational clusters that make up 99% of the trajectory of the unrestrained* (left column) *and NOE distance-restrained* (right column) *simulations of compounds* **3** (upper panels) *and* **8** (lower panels)

In the case of compound **8** (*Fig. 10*), both simulations have sampled a relatively small part of conformational space; the most populated cluster has a presence of 53 and 95% in the unrestrained and NOE-restrained simulation, respectively, and their helical conformations are rather similar (*Figs. 11* and *12*). Although both peptides contain the same number of α- and β-residues, compound **8** samples a much smaller part of their conformational spaces (see *Fig. 7*). This figure also shows that NOE distance restraining reduces the sampling considerably.

Conclusions. – The conformational behavior of two heptapeptides consisting of α- and β-residues, which adopt different folded conformations in MeOH has been

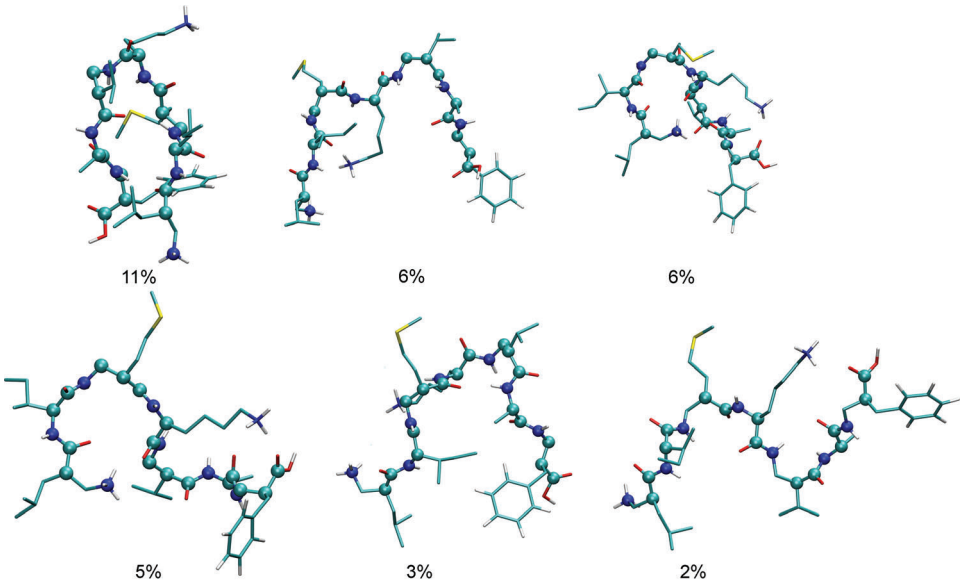

Fig. 8. *Central structures of the six most populated clusters in the 80-ns-long unrestrained simulation of compound* **3** *with their populations*

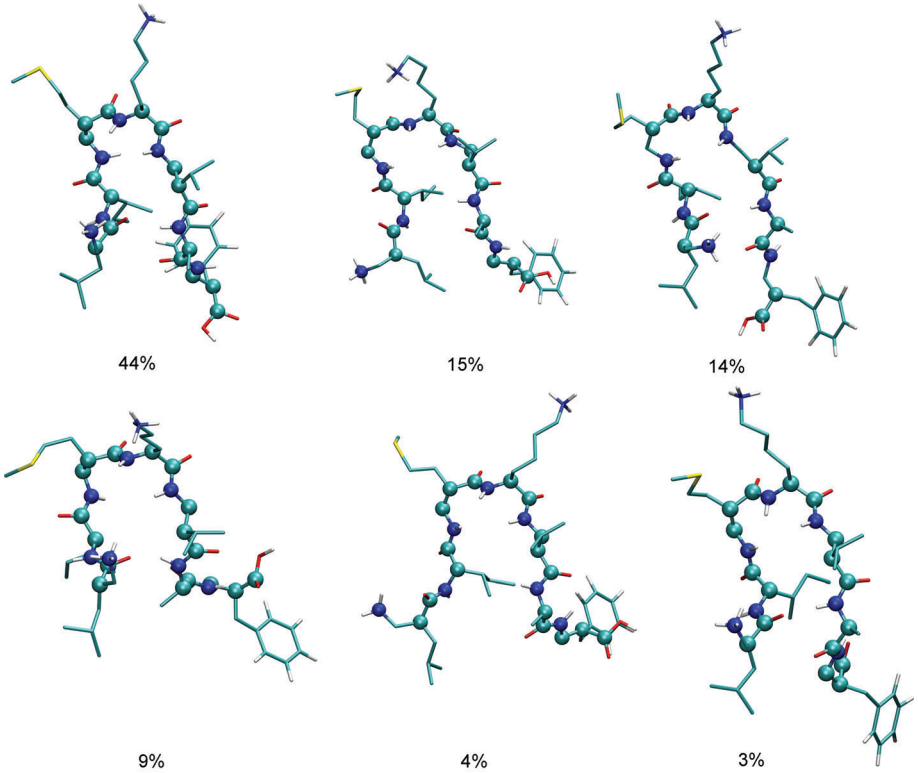

Fig. 9. *Central structures of the six most populated clusters in the first 40 ns of the NOE-restrained simulation of compound* **3** *with their populations*

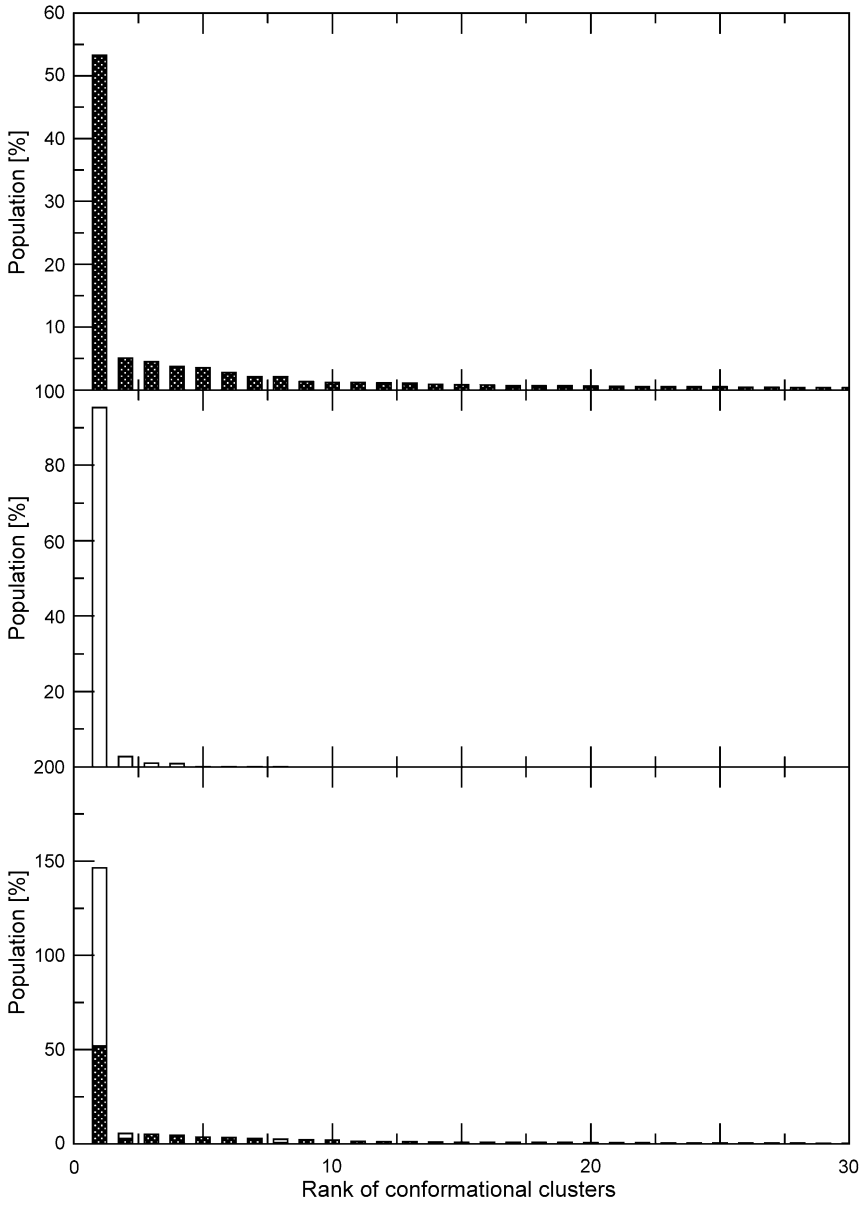

Fig. 10. *Compound* **8**: *conformational clustering of the 40-ns trajectories of the unrestrained simulation* (upper panel), *of the NOE-restrained simulation* (middle panel), *and of the combined trajectories of these two simulations* (lower panel)

investigated by means of MD simulations using the recently proposed GROMOS force-field parameter set 54A7 for biomolecules. The available experimental data, 38 NOE atom–atom distance bounds and nine $^3J(H_N,H_{\alpha/\beta})$ couplings for peptide **3** that

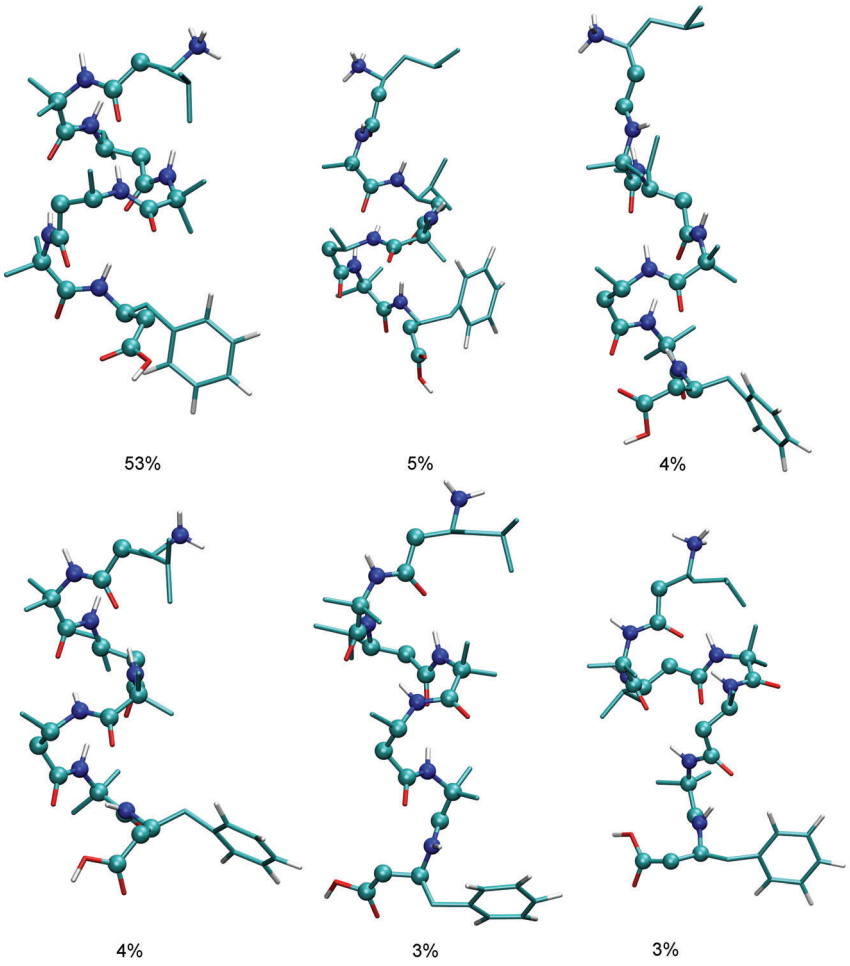

Fig. 11. *Central structures of the six most populated clusters in the 80 ns of the unrestrained simulation of compound* **8** *with their populations*

lead to a hairpin-like dominant fold, and 53 NOE atom–atom distance bounds and three $^{3}J(H_{N}H_{\alpha/\beta})$ couplings for peptide **8** that define a helical dominant fold, are largely reproduced in the unrestrained MD simulations.

For peptide **3**, only three NOE distance bounds are violated by up to 0.27 nm. These three NOEs define alternative conformations of the residues involved in the hairpin. Application of NOE-distance restraining during the MD simulation generates a conformational ensemble that agrees with the experimental data and is different from that generated in the unrestrained simulation. The NOE-distance-restrained conformational ensemble does not confirm the nine-membered ring conformation formed by the H-bond β^{2}Met3 H:Lys4O proposed earlier based on the experimental data. Since for peptide **3** only four NOE distance bounds involve atoms in residues not adjacent in the

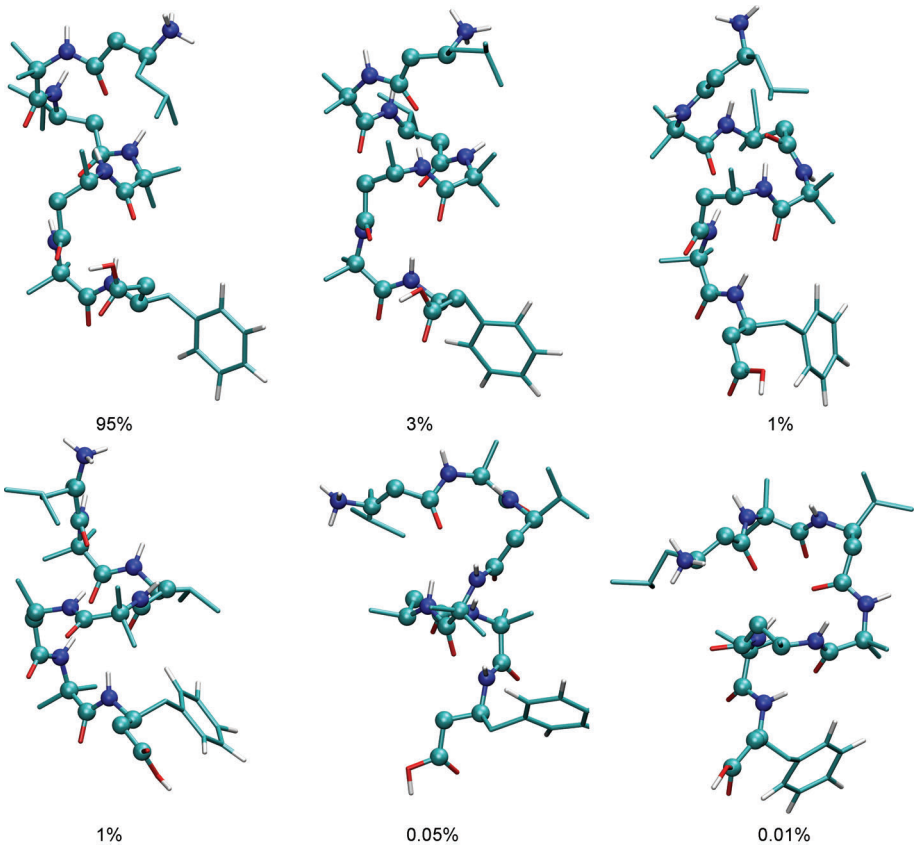

Fig. 12. *Central structures of the six most populated clusters in the 40-ns-long NOE-restrained simulation of compound* **8** *with their populations*

residue sequence, the NOE restraints leave the peptide a rather large conformational freedom.

For peptide **8**, only two NOE distance bounds are violated by up to 0.18 nm. These two NOEs involve residue β^3Leu1 which is not involved in H-bonds, characterizing the dominant helical conformation. Application of NOE distance restraining during the MD simulation generates a conformational ensemble that agrees with the experimental data, but is essentially reduced to a single helical conformation.

The GROMOS 54A7 force field reproduces the dominant hairpin and helical folds for peptides **3** and **8**, respectively, but, according to the experimental data, these conformations should be slightly more stable. The results indicate that the 54A7 force field can be favorably used in MD simulations or structure refinement of mixed α/β-peptides in MeOH solution.

The authors thank the *Swiss National Science Foundation*, grant No. 200021-137827, and its *National Competence Center for Research* (NCCR) in Structural Biology, and the *European Research Council*, grant No. 228076, for financial support.

REFERENCES

[1] S. H. Gellman, *Acc. Chem. Res.* **1998**, *31*, 173.
[2] D. Seebach, S. Abele, J. V. Schreiber, B. Martinoni, A. K. Nussbaum, H. Schild, H. Schulz, H. Hennecke, R. Woessner, F. Bitsch, *Chimia* **1998**, *52*, 734.
[3] R. P. Cheng, S. H. Gellman, W. F. DeGrado, *Chem. Rev.* **2001**, *101*, 3219.
[4] D. L. Steer, R. A. Lew, P. Perlmutter, A. I. Smith, M. I. Aguilar, *Curr. Med. Chem.* **2002**, *9*, 811.
[5] D. F. Hook, F. Gessier, C. Noti, P. Kast, D. Seebach, *ChemBioChem* **2004**, *5*, 691.
[6] D. Seebach, K. Gademann, J. V. Schreiber, J. L. Matthews, T. Hintermann, B. Jaun, L. Oberer, U. Hommel, H. Widmer, *Helv. Chim. Acta* **1997**, *80*, 2033.
[7] D. H. Appella, L. A. Christianson, D. A. Klein, M. R. Richards, D. R. Powell, S. H. Gellman, *J. Am. Chem. Soc.* **1999**, *121*, 7574.
[8] M. A. Schmitt, S. H. Choi, I. A. Guzei, S. H. Gellman, *J. Am. Chem. Soc.* **2005**, *127*, 13130.
[9] D. F. Hook, P. Bindschädler, Y. R. Mahajan, R. Šebesta, P. Kast, D. Seebach, *Chem. Biodiversity* **2005**, *2*, 591.
[10] A. Hayen, M. A. Schmitt, F. N. Ngassa, K. A. Thomasson, S. H. Gellman, *Angew. Chem., Int. Ed.* **2004**, *43*, 505.
[11] S. De Pol, C. Zorn, C. D. Klein, O. Zerbe, O. Reiser, *Angew. Chem., Int. Ed.* **2004**, *43*, 511.
[12] R. S. Roy, I. L. Karle, S. Raghothama, P. Balaram, *Proc. Natl. Acad. Sci. U.S.A.* **2004**, *101*, 16478.
[13] K. Ananda, P. G. Vasudev, A. Sengupta, K. M. P. Raja, N. Shamala, P. Balaram, *J. Am. Chem. Soc.* **2005**, *127*, 16668.
[14] G. V. M. Sharma, P. Nagendar, P. Jayaprakash, P. R. Krishna, K. V. S. Ramakrishna, A. C. Kunwar, *Angew. Chem., Int. Ed.* **2005**, *44*, 5878.
[15] M. A. Schmitt, S. H. Choi, I. A. Guzei, S. H. Gellman, *J. Am. Chem. Soc.* **2006**, *128*, 4538.
[16] D. Seebach, B. Jaun, R. Sebesta, R. I. Mathad, O. Flögel, M. Limbach, H. Sellner, S. Cottens, *Helv. Chim. Acta* **2006**, *89*, 1801.
[17] D. Trzesniak, A. Glättli, B. Jaun, W. F. van Gunsteren, *J. Am. Chem. Soc.* **2005**, *127*, 14320.
[18] W. F. van Gunsteren, Z. Gattin, in 'Foldamers: Structure, Properties and Applications', Eds. S. Hecht, I. Huc, Wiley-VCH, Weinheim, Germany, 2007, Chapt. 6, p. 173.
[19] Z. Gattin, A. Glättli, B. Jaun, W. F. van Gunsteren, *Biopolymers* **2007**, *85*, 318.
[20] Y.-D. Wu, D.-P. Wang, *J. Am. Chem. Soc.* **1998**, *120*, 13485.
[21] Y. D. Wu, D. P. Wang, *J. Am. Chem. Soc.* **1999**, *121*, 9352.
[22] X. Zhu, A. Yethiraj, Q. Cui, *J. Chem. Theory Comput.* **2007**, *3*, 1538.
[23] A. Warshel, 'Computer modeling of chemical reactions in enzymes and solutions', John Wiley and Sons, New York, 1997.
[24] M. Karplus, J. A. McCammon, *Nat. Struct. Biol.* **2002**, *9*, 646; corrigendum: *Nat. Struct. Biol.* **2002**, *9*, 788.
[25] S. A. Adcock, J. A. McCammon, *Chem. Rev.* **2006**, *106*, 1589.
[26] W. F. van Gunsteren, D. Bakowies, R. Baron, I. Chandrasekhar, M. Christen, X. Daura, P. Gee, D. P. Geerke, A. Glättli, P. H. Hünenberger, M. A. Kastenholz, C. Oostenbrink, M. Schenk, D. Trzesniak, N. F. A. van der Vegt, H. B. Yu, *Angew. Chem., Int. Ed.* **2006**, *45*, 4064.
[27] R. L. Baldwin, *J. Mol. Biol.* **2007**, *371*, 283.
[28] W. F. van Gunsteren, J. Dolenc, A. E. Mark, *Curr. Opin. Struct. Biol.* **2008**, *18*, 149.
[29] W. F. van Gunsteren, J. Dolenc, *Biochem. Soc. Trans.* **2008**, *36*, 11.
[30] D. Poger, W. F. van Gunsteren, A. E. Mark, *J. Comput. Chem.* **2010**, *31*, 1117.
[31] N. Schmid, A. P. Eichenberger, A. Choutko, S. Riniker, M. Winger, A. E. Mark, W. F. van Gunsteren, *Eur. Biophys. J. Biophys. Lett.* **2011**, *40*, 843.
[32] http://www.gromos.net.
[33] W. Huang, Z. Lin, W. F. van Gunsteren, *J. Chem. Theory Comput.* **2011**, *7*, 1237.
[34] C. Oostenbrink, A. Villa, A. E. Mark, W. F. van Gunsteren, *J. Comput. Chem.* **2004**, *25*, 1656.
[35] L. D. Schuler, X. Daura, W. F. van Gunsteren, *J. Comput. Chem.* **2001**, *22*, 1205.
[36] A. E. Torda, R. M. Scheek, W. F. van Gunsteren, *J. Mol. Biol.* **1990**, *214*, 223.
[37] R. Walser, A. E. Mark, W. F. van Gunsteren, M. Lauterbach, G. Wipff, *J. Chem. Phys.* **2000**, *112*, 10450.

[38] N. Schmid, J. R. Allison, J. Dolenc, A. P. Eichenberger, A.-P. E. Kunz, W. F. van Gunsteren, *J. Biomol. NMR* **2011**, *51*, 265.
[39] J.-P. Ryckaert, G. Ciccotti, H. J. C. Berendsen, *J. Comput. Phys.* **1977**, *23*, 327.
[40] J. A. Barker, R. O. Watts, *Mol. Phys.* **1973**, *26*, 789.
[41] I. G. Tironi, R. Sperb, P. E. Smith, W. F. van Gunsteren, *J. Chem. Phys.* **1995**, *102*, 5451.
[42] H. J. C. Berendsen, J. P. M. Postma, W. F. van Gunsteren, A. DiNola, J. R. Haak, *J. Chem. Phys.* **1984**, *81*, 3684.
[43] X. Daura, W. F. van Gunsteren, A. E. Mark, *Proteins* **1999**, *34*, 269.
[44] K. Wüthrich, M. Billeter, W. Braun, *J. Mol. Biol.* **1983**, *169*, 949.
[45] W. F. van Gunsteren, S. R. Billeter, A. A. Eising, P. H. Hünenberger, P. Krüger, A. E. Mark, W. R. P. Scott, I. G. Tironi, 'Biomolecular Simulation: The GROMOS96 Manual and User Guide', vdf Hochschulverlag, ETH Zurich, 1996.
[46] M. Karplus, *J. Chem. Phys.* **1959**, *30*, 11.
[47] M. Karplus, *J. Am. Chem. Soc.* **1963**, *85*, 2870.
[48] A. Pardi, M. Billeter, K. Wüthrich, *J. Mol. Biol.* **1984**, *180*, 741.
[49] D. Steiner, J. R. Allison, A. P. Eichenberger, W. F. van Gunsteren, *J. Biomol. NMR* **2012**, *53*, 223.

Received September 17, 2012